ARL-RP-0564 ● MAR 2016

US Army Research Laboratory

Longitudinal Impact of Piezoelectric Media

by George A Gazonas, Raymond A Wildman, David A Hopkins, and Michael J Scheidler

A reprint from Arch Appl Mech. 2016;86:497–515.

Approved for public release; distribution unlimited.

NOTICES

Disclaimers

The findings in this report are not to be construed as an official Department of the Army position unless so designated by other authorized documents.

Citation of manufacturer's or trade names does not constitute an official endorsement or approval of the use thereof.

Destroy this report when it is no longer needed. Do not return it to the originator.

ARL-RP-0564 ● MAR 2016

US Army Research Laboratory

Longitudinal Impact of Piezoelectric Media

by George A Gazonas, Raymond A Wildman, and David A Hopkins
Weapons and Materials Research Directorate, ARL

Michael J Scheidler
ARL Guest Researcher

A reprint from Arch Appl Mech. 2016;86:497–515.

Approved for public release; distribution unlimited.

REPORT DOCUMENTATION PAGE

Form Approved
OMB No. 0704-0188

Public reporting burden for this collection of information is estimated to average 1 hour per response, including the time for reviewing instructions, searching existing data sources, gathering and maintaining the data needed, and completing and reviewing the collection information. Send comments regarding this burden estimate or any other aspect of this collection of information, including suggestions for reducing the burden, to Department of Defense, Washington Headquarters Services, Directorate for Information Operations and Reports (0704-0188), 1215 Jefferson Davis Highway, Suite 1204, Arlington, VA 22202-4302. Respondents should be aware that notwithstanding any other provision of law, no person shall be subject to any penalty for failing to comply with a collection of information if it does not display a currently valid OMB control number.
PLEASE DO NOT RETURN YOUR FORM TO THE ABOVE ADDRESS.

1. REPORT DATE *(DD-MM-YYYY)*	2. REPORT TYPE	3. DATES COVERED (From - To)
March 2016	Reprint	March 2014 – April 2015

4. TITLE AND SUBTITLE
Longitudinal Impact of Piezoelectric Media

5a. CONTRACT NUMBER

5b. GRANT NUMBER

5c. PROGRAM ELEMENT NUMBER

6. AUTHOR(S)
George A Gazonas, Raymond A Wildman, David A Hopkins, and Michael J Scheidler

5d. PROJECT NUMBER
AH-84

5e. TASK NUMBER

5f. WORK UNIT NUMBER

7. PERFORMING ORGANIZATION NAME(S) AND ADDRESS(ES)
US Army Research Laboratory
ATTN: RDRL-WMM-B
Aberdeen Proving Ground, MD 21005-5069

8. PERFORMING ORGANIZATION REPORT NUMBER
ARL-RP-0564

9. SPONSORING/MONITORING AGENCY NAME(S) AND ADDRESS(ES)

10. SPONSOR/MONITOR'S ACRONYM(S)

11. SPONSOR/MONITOR'S REPORT NUMBER(S)

12. DISTRIBUTION/AVAILABILITY STATEMENT
Approved for public release; distribution is unlimited.

13. SUPPLEMENTARY NOTES
A reprint from Arch Appl Mech. 2016;86:497–515.

14. ABSTRACT
We consider the elastodynamic impact problem involving a one-dimensional finite-thickness piezoelectric flyer traveling at initial velocity V_0 that collides with (and adheres to) a stationary piezoelectric target of finite thickness backed by a semi-infinite non-piezoelectric elastic half-space.We derive expressions for the stress, velocity, and electric displacement in the target at all times after impact. A combined d'Alembert and Laplace transform method is used to derive new numerically based solutions for this class of transient wave propagation problems. A modified Dubner–Abate–Crump (DAC) algorithm is used to invert the analytical Laplace transform domain solutions to the time domain. Unlike many authors who neglect electromechanical coupling in the initially unstressed region ahead of the shock, we consider this effect, which gives rise to the development of a tensile stress wave within the piezoelectric target ahead of the shock. To solve the problem, we derive a new piezoelectric impact boundary condition and apply it to the problem of a finite quartz (SiO_2) flyer impacting a lead zirconate titanate (PZT-4) target and find that the solutions obtained using the modified DAC algorithm compare well with those obtained using both a finite-difference time-domain method, and the commercial finite element code, COMSOL multiphysics.

15. SUBJECT TERMS
1-D elastodynamics; Numerical inverse Laplace transform; Mathematica source code; d'Alembert method; Dubner–Abate–Crump

16. SECURITY CLASSIFICATION OF:			17. LIMITATION OF ABSTRACT	18. NUMBER OF PAGES	19a. NAME OF RESPONSIBLE PERSON
					George A Gazonas
a. REPORT	b. ABSTRACT	c. THIS PAGE			19b. TELEPHONE NUMBER (Include area code)
Unclassified	Unclassified	Unclassified	UU	24	410-306-0863

Standard Form 298 (Rev. 8/98)
Prescribed by ANSI Std. Z39.18

Arch Appl Mech (2016) 86:497–515
DOI 10.1007/s00419-015-1042-3

ORIGINAL

George A. Gazonas · Raymond A. Wildman · David A. Hopkins · Michael J. Scheidler

Longitudinal impact of piezoelectric media

Received: 16 April 2015 / Accepted: 9 July 2015 / Published online: 25 July 2015
© Springer-Verlag Berlin Heidelberg (outside the USA) 2015

Abstract We consider the elastodynamic impact problem involving a one-dimensional finite-thickness piezoelectric flyer traveling at initial velocity V_0 that collides with (and adheres to) a stationary piezoelectric target of finite thickness backed by a semi-infinite non-piezoelectric elastic half-space. We derive expressions for the stress, velocity, and electric displacement in the target at all times after impact. A combined d'Alembert and Laplace transform method is used to derive new numerically based solutions for this class of transient wave propagation problems. A modified Dubner–Abate–Crump (DAC) algorithm is used to invert the analytical Laplace transform domain solutions to the time domain. Unlike many authors who neglect electromechanical coupling in the initially unstressed region ahead of the shock, we consider this effect, which gives rise to the development of a tensile stress wave within the piezoelectric target ahead of the shock. To solve the problem, we derive a new piezoelectric impact boundary condition and apply it to the problem of a finite quartz (SiO_2) flyer impacting a lead zirconate titanate (PZT-4) target and find that the solutions obtained using the modified DAC algorithm compare well with those obtained using both a finite-difference time-domain method, and the commercial finite element code, COMSOL multiphysics.

Keywords 1-D elastodynamics · Numerical inverse Laplace transform · Mathematica source code · d'Alembert method · Dubner–Abate–Crump

1 Introduction

Much of the literature that presents analytical or computational solutions to "impact-type" initial boundary value problems assumes an impact boundary condition in the form of a constant applied step in stress or velocity, cf. [1–3]. This simplifying assumption is particularly useful for characterizing elastic shocks in flyers and targets that are homogeneous, linear elastic, and semi-infinite. Here, elastic shocks are defined by stress

G. A. Gazonas (✉) · R. A. Wildman · D. A. Hopkins · M. J. Scheidler
U.S. Army Research Laboratory, ATTN: RDRL-WMM-B, Aberdeen Proving Ground, MD 21005-5069, USA
E-mail: george.a.gazonas.civ@mail.mil
Tel.: 410-306-0863
Fax: 410-306-0759

R. A. Wildman
E-mail: raymond.a.wildman.civ@mail.mil

D. A. Hopkins
E-mail: david.a.hopkins.civ@mail.mil

M. J. Scheidler
E-mail: michael.j.scheidler2.ctr@mail.mil

waves with amplitudes that are less than or equal to the Hugoniot elastic limit, cf. p. 248, equation (10.4) of Davison [4]. However, during the collision of piezoelectric media that are multilayered, or inhomogeneous, or possess other material discontinuities, the target (and possibly flyer) introduce multiply-reflected or scattered waves at the impact face, so that the history of the stress σ and the particle velocity v at the impact face is generally time-dependent, not constant, and cannot be known in advance of the solution to the problem. Thus, the widespread use of a constant stress or velocity boundary condition in the mechanics literature is an invalid assumption for modeling impact in such media.

Both Redwood [5] and Steutzer [6] study the problem of multiply-reflected transient waves, characterized by an infinite set of jump discontinuities, in linear piezoelectrics subjected to either a step in stress or voltage. These boundary conditions, however, are not appropriate for the piezoelectric impact problem. Other works address shock wave propagation in *nonlinear* piezoelectric media [7–9], but the complexity of the material response prohibits an analytical treatment of the electromechanical coupling in the unstressed region ahead of the shock wave.

For engineering applications, our problem is applicable to either a uniaxial (or 1-D) Kolsky bar or plate impact experiment conducted at stress levels below the Hugoniot elastic limit. In these experiments, flyer, target or both can be composed of piezoelectric material. Apart from these experimental applications, the solutions derived in this paper can be used to verify large-scale computational simulations of impact phenomena involving piezoelectric media. Indeed, the COMSOL multiphysics commercial finite element code and a finite-difference time-domain (FDTD) computational code have been verified with the piezoelectric numerical solutions presented in this paper; these codes can now be used with more confidence for solving more complex 2-D or 3-D geometries where piezoelectric impact solutions (albeit numerical) may not be available for code verification.

We first present the linear equations of dynamic piezoelectricity, following closely the development found in Redwood [5] and Steutzer [6], and show how the d'Alembert solution is also applicable to the study of multiply-reflected transient waves in linear piezoelectrics subjected to impact. The problem of a semi-infinite elastic flyer impacting a finite elastic target backed by a semi-infinite elastic half-space was addressed in [10], and the problem of a semi-infinite elastic flyer impacting a finite piezoelectric target backed by an elastic half-space was addressed in [11]. Most similar to our own study is the work of Le [12,13] who uses the method of characteristics to determine exact solutions to the problem of a finite-length piezoceramic rod, traveling at an initial constant velocity, that impacts a second, identical, but stationary piezoceramic rod; Le [12,13] derives exact solutions for electric displacement and stress, up until the first wave reflection, for the case when the external ends of the rods are electrically short-circuited.

In the current study, we consider the one-dimensional (1-D) normal impact problem in which a finite piezoelectric flyer collides with a finite, stationary piezoelectric target bonded to a semi-infinite elastic half-space. Here, a new impact boundary condition is derived, based on the d'Alembert solution to the wave equation. Our results are analytical in the Laplace transform domain but are numerically inverted to the time domain using a Dubner–Abate–Crump (DAC) algorithm [14–16], modified in [17] (using Lanczos σ-factors) to mitigate the effects of the Gibbs phenomenon (ringing seen in Fourier series representations of jump discontinuities). The use of the DAC algorithm for solution of transient wave propagation problems has seen a resurgence in the recent mechanics literature [18–20], but other than our own prior work [11,21], we are not aware of applications of the DAC algorithm to collision phenomena, i.e., impact.

The remainder of the paper is organized as follows. Section 2 briefly discusses the 1-D constitutive equations and plane wave propagation in a linear piezoelectric medium. Section 3 describes the d'Alembert solution to the wave equation in the target with homogeneous initial conditions. Section 4 contains our derivation of a new impact boundary condition for a finite piezoelectric flyer, which utilizes the d'Alembert solution of the wave equation in the flyer. In Sect. 5, we present additional boundary and electrical conditions necessary to determine the stress, particle velocity and electrical displacement in the target for all time. The Laplace transform is used in Sect. 6 to convert time derivatives of the boundary, stress continuity, and electrical conditions on the flyer and target into algebraic functions of the Laplace transform domain variable s. Laplace transform of the impact boundary condition results in an integral equation which can be solved explicitly. Here, it is also shown how the impact boundary condition for a finite-thickness piezoelectric flyer specializes to that of a finite-thickness elastic flyer and further to that of a semi-infinite elastic flyer. Section 7 contains plots of the stress, particle velocity, and electrical displacement at the midpoint of a lead zirconate titanate (PZT-4) target under impact by a quartz (SiO_2) flyer. For comparison with the numerical inverse Laplace transform solutions, the figures also include numerical solutions using a COMSOL multiphysics finite element solution and a FDTD method. We close with a discussion which outlines the major results of the paper. "Appendix 1" contains Laplace transform

domain functions $\overline{F}_1(s)$, $\overline{G}_1(s)$, and $\overline{D}_1(s)$ used to numerically determine the stress, particle velocity, and electric displacement in the target using the numerical inverse Laplace transform (ILT) Mathematica source code listed in "Appendix 2." "Appendix 2" also includes a stress time history plot (Fig. 5) at the center of a target under impact by a flyer. Both the flyer and target are composed of synthetic elastic and piezoelectric materials and accentuate the differences between the various numerical (ILT, FDTD, FE) methods used to solve the impact problem. Finally, in "Appendix 3" we compute the relative error between our numerical ILT-derived solution and the exact analytical solution derived by Le [12,13] for the case of a finite-length piezoceramic rod, traveling at an initial constant velocity, that impacts a second, identical, but stationary piezoceramic rod; here, it is shown that the numerical ILT solutions are quite accurate over the impact interval $0 \leq t \leq 2l/c$.

2 Plane waves in piezoelectric media

The 1-D constitutive equations for a linear piezoelectric material can be written as [5,25]

$$\sigma(x,t) = \pm\left[C^D \frac{\partial u(x,t)}{\partial x} - hD(x,t)\right], \tag{1}$$

$$\mathscr{E}(x,t) = -h\frac{\partial u(x,t)}{\partial x} + D(x,t)/\varepsilon. \tag{2}$$

σ is the stress in N/m^2; the upper "+" sign in Eq. (1) corresponds to the convention that stress is positive in tension and the lower "−" sign that stress is positive in compression. C^D is Young's modulus measured at constant D in N/m^2, u is the particle displacement in m measured at point x relative to the undeformed configuration at time t in s measured from the time of impact at $t = 0$. D is the electric flux density (or electric displacement) in C/m^2, $\varepsilon = \varepsilon_0\,\varepsilon_r$ is the dielectric permittivity in F/m, ε_0 is the permittivity of a vacuum in F/m, ε_r is the relative permittivity of the medium, h is a piezoelectric constant measured at constant D in V/m, and $\mathscr{E}$ is the electric field in V/m (or N/C). The piezoelectrically stiffened elastic constant C^D in Eq. (1) is defined in Cady [24] [p. 270 equation (271 a)], by the Institute of Radio Engineers (IRE) [25] (p. 1394, Table III) or Chen et al. [1] (p. 4760) and is given by

$$C^D = C^E + e\,h, \tag{3}$$

where C^E is Young's modulus measured at constant $\mathscr{E}$, e is a piezoelectric coupling constant in C/m^2, and $h = e/\varepsilon$. In addition, momentum balance yields

$$\rho\frac{\partial v(x,t)}{\partial t} = \pm\frac{\partial \sigma(x,t)}{\partial x}, \tag{4}$$

where ρ is the mass density in kg/m^3 and $v(x,t)$ is the particle velocity

$$v(x,t) = \frac{\partial u(x,t)}{\partial t}. \tag{5}$$

Following the development in Redwood [5] or Steutzer [6] for linear piezoelectric media, substitution of Eqs. (1) and (5) into Eq. (4) gives

$$\frac{\partial^2 u(x,t)}{\partial t^2} = \frac{C^D}{\rho}\frac{\partial^2 u(x,t)}{\partial x^2} - \frac{h}{\rho}\frac{\partial D(x,t)}{\partial x}. \tag{6}$$

If there is no free charge, $\rho_{\text{free}} = 0$, inside the piezoelectric medium, then (see e.g., Lorrain and Corson [26], p. 109)

$$\frac{\partial D(x,t)}{\partial x} = div\ D = \rho_{\text{free}} = 0. \tag{7}$$

The time-varying electric displacement D, therefore, is at most spatially uniform, that is, a function of time only, so we can write $D(x,t) = D(t)$, and Eq. (6) becomes

$$\frac{\partial^2 u(x,t)}{\partial t^2} = c^2\frac{\partial^2 u(x,t)}{\partial x^2}, \tag{8}$$

where $c = \sqrt{C^D/\rho}$ is the piezo-modified longitudinal wave speed with C^D given by Eq. (3). Observe that (8) does not depend upon the sign convention for the stress.

In the sequel below, we denote material constants and field variables in the piezoelectric target with a subscript of "1", and subscripts of "0" and "h" refer to quantities in the piezoelectric flyer and elastic half-space, respectively. We also remark that the electric displacement D is continuous across material interfaces, cf. p. 140 of [26], so that at the boundary $x = 0$ between the flyer and target $D_0(t) = D_1(t)$; if the electric displacement is spatially uniform in both the flyer and target and equal at the impact face, then the electric displacement is spatially uniform in both the flyer and target. Furthermore, any jump $[\![\ \ ]\!]$ in electric displacement across an elastic shock, moving at velocity c_0 or c_1, within either the flyer or target is identically zero, i.e., $[\![D_0]\!](t) = [\![D_1]\!](t) = \sigma_{\mathrm{f}} = 0$, since the surface charge density σ_{f} is identically zero on the shock front.[1]

3 Impact-induced plane waves in a piezoelectric target

We now consider the problem of a piezoelectric flyer of finite thickness k traveling at initial velocity V_0 that collides with (and adheres to) an undeformed, stationary piezoelectric target of finite thickness l; the target is backed by a semi-infinite non-piezoelectric elastic half-space (Fig. 1). Henceforth, we assume that stress is taken positive in compression, so that the stress σ_1 in the linear elastic piezoelectric target is given by Eq. (1) with the minus sign:

$$\sigma_1(x,t) = -C_1^D \frac{\partial u_1(x,t)}{\partial x} + h_1 D_1(t). \tag{9}$$

The transient target displacements $u_1(x,t)$ are governed by the wave equation (8) in one-spatial dimension

$$\frac{\partial^2 u_1(x,t)}{\partial t^2} = c_1^2 \frac{\partial^2 u_1(x,t)}{\partial x^2} \quad \text{for} \quad 0 < x < l, \quad t > 0. \tag{10}$$

The general solution to the wave Eq. (10) in the target can be constructed using d'Alembert's relation:

$$u_1(x,t) = f_1(t - x/c_1) + g_1(t + x/c_1), \tag{11}$$

where $f_1(\cdot)$ and $g_1(\cdot)$ are arbitrary functions. The displacement u_1 is assumed to be continuous and piecewise smooth, which implies that the d'Alembert functions f_1 and g_1 are also continuous and piecewise smooth. Letting f_1 and g_1 denote the antiderivatives of F_1 and G_1, respectively, i.e., $f_1' = F_1$ and $g_1' = G_1$, then the d'Alembert solution (11), together with the Eq. (9) for the stress in the target, yields

$$\sigma_1(x,t) = z_1\Big[F_1(t - x/c_1) - G_1(t + x/c_1)\Big] + h_1 D_1(t), \tag{12}$$

where $z_1 = \rho_1 c_1$ is the piezo-modified target impedance. Similarly, the particle velocity v_1 in the target is given by

$$v_1(x,t) = \frac{\partial u_1}{\partial t} = F_1(t - x/c_1) + G_1(t + x/c_1). \tag{13}$$

It is evident that the stress and particle velocity in the target are determined once the functions F_1, G_1, and D_1 are determined. Note that discontinuities in F_1 or G_1 correspond to the passage of shock waves at interior points or the reflection of shock waves at the boundaries $x = 0$ and $x = l$.

To solve for F_1, G_1, and D_1 requires consideration of the initial conditions (in this case homogeneous) and boundary conditions of the target. The initial conditions in the target are

$$u_1(x,0) = 0, \quad \frac{\partial u_1(x,0)}{\partial t} = v_1(x,0) = 0 \quad \text{for} \quad 0 \le x \le l. \tag{14}$$

Furthermore, Eq. $(14)_1$ and the stress–strain Eq. (9) implies that for a stress-free initial state in the target that

$$\sigma_1(x,0) = D_1(0) = 0 \quad \text{for} \quad 0 \le x \le l. \tag{15}$$

[1] Electrodynamic jump conditions for moving boundaries are derived in [27], cf. p. 1187, Table 1.

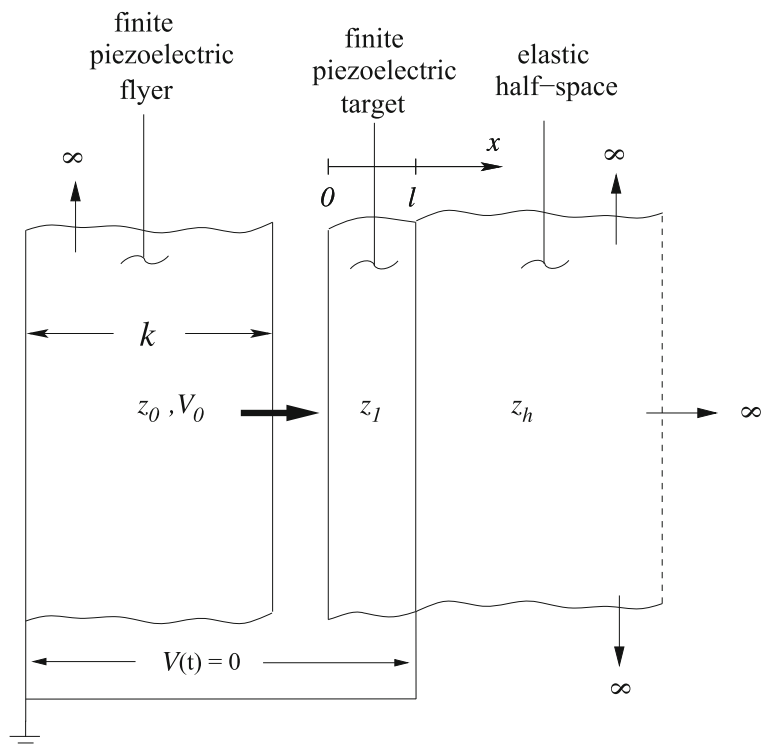

Fig. 1 A finite piezoelectric flyer (thickness k and impedance z_0) traveling at initial velocity V_0 impacting a finite and stationary piezoelectric target (thickness l and impedance z_1); the short-circuited flyer and target voltage $V(t) = 0$ is backed by a semi-infinite non-piezoelectric elastic half-space (impedance z_h)

4 Impact boundary condition for a finite piezoelectric flyer

We wish to derive a relationship between stress σ, velocity v, and electric displacement D at the impact face $x = 0$. The derivation of this boundary condition for a finite piezoelectric flyer that impacts a finite, but stationary, piezoelectric target at the instant $t = 0$ follows closely the derivation of the impact boundary condition for the elastodynamic impact problem studied in [10]. Two important differences in this work from the problem studied in [10] are that, in this work, the flyer has finite thickness k and is piezoelectric.

The initial conditions in the flyer are

$$v_0(x, 0) = V_0 > 0, \quad \text{and} \quad \sigma_0(x, 0) = D_0(0) = 0 \quad \text{for} \quad -k \leq x \leq 0. \tag{16}$$

The stress-free boundary condition at $x = -k$ (Fig. 1) is

$$\sigma_0(-k, t) = 0 \quad \text{for} \quad t \geq 0. \tag{17}$$

Analogous to Eqs. (12) and (13) for the target, the normalized stress, taken positive in compression, in the flyer can be written as

$$\frac{\sigma_0(x, t)}{z_0} = F_0(t - x/c_0) - G_0(t + x/c_0) + \frac{h_0}{z_0} D_0(t), \tag{18}$$

and the velocity in the flyer can be written as

$$v_0(x, t) = \frac{\partial u_0}{\partial t} = F_0(t - x/c_0) + G_0(t + x/c_0). \tag{19}$$

It is apparent that functions F_0 and G_0 have dimensions of velocity.

Let t_* denote the travel time in the flyer, that is, the time it takes for the shock wave to travel the length k of the finite flyer:

$$t_* = \frac{k}{c_0}. \tag{20}$$

Further, we define a non-dimensional distance y and time τ by

$$y \equiv \frac{x}{k} = \frac{x}{c_0 t_*}, \quad \tau \equiv \frac{t}{t_*} = \frac{c_0 t}{k}, \quad \text{for } (y, \tau) \in [-1, 0] \times [0, \infty), \tag{21}$$

such that the shock wave requires the non-dimensional time $\tau = 1$ to travel the non-dimensional length $y = 1$ of the flyer. Since

$$\frac{x}{c_0} = \frac{ky}{k/t_*} = t_* y, \tag{22}$$

we see that the argument of functions F_0 and G_0 appearing in Eqs. (18) and (19) can be replaced by any of the following expressions:

$$t \pm x/c_0 = t_* \tau \pm t_* y = t_*(\tau \pm y). \tag{23}$$

Therefore, if we let

$$F(w) \equiv F_0(t_* w), \quad G(w) \equiv G_0(t_* w), \tag{24}$$

and

$$v_*(y, \tau) = v_0(x, t), \quad \sigma_*(y, \tau) = \frac{\sigma_0(x, t)}{z_0}, \quad D_*(\tau) = \frac{h_0}{z_0} D_0(t), \tag{25}$$

we can rewrite Eq. (18) as

$$\sigma_*(y, \tau) = F(\tau - y) - G(\tau + y) + D_*(\tau), \tag{26}$$

and Eq. (19) as

$$v_*(y, \tau) = F(\tau - y) + G(\tau + y), \quad \text{for } (y, \tau) \in [-1, 0] \times [0, \infty). \tag{27}$$

Therefore, the domains of d'Alembert functions F and G are, $F \in [0, \infty)$ and $G \in [-1, \infty)$. The initial conditions (16) can be rewritten in the non-dimensional form

$$v_*(y, 0) = V_0, \quad \sigma_*(y, 0) = D_*(0) = 0 \quad -1 \le y \le 0. \tag{28}$$

Similarly, the stress-free boundary condition (17) can be rewritten in the non-dimensional form

$$\sigma_*(-1, \tau) = 0, \quad \tau \ge 0. \tag{29}$$

On setting $\tau = 0$ in (26) and (27) and using initial conditions (28), we obtain

$$F(-y) + G(y) = V_0, \quad -1 \le y \le 0, \tag{30}$$

and

$$F(-y) - G(y) = 0, \quad -1 \le y \le 0. \tag{31}$$

Therefore,

$$G(y) = F(-y) = \frac{1}{2} V_0, \quad -1 \le y \le 0, \tag{32}$$

or

$$F(w) = \frac{1}{2} V_0, \quad 0 \le w \le 1. \tag{33}$$

On setting $y = -1$ in Eq. (26) and using Eq. (29), we obtain

$$0 = \sigma_*(-1, \tau) = F(\tau + 1) - G(\tau - 1) + D_*(\tau), \quad \tau \geq 0, \tag{34}$$

which when solved for F yields

$$F(\tau + 1) = G(\tau - 1) - D_*(\tau), \quad \tau \geq 0. \tag{35}$$

Letting $\tau = w - 1$ in (35) yields

$$F(w) = G(w - 2) - D_*(w - 1), \quad w \geq 1. \tag{36}$$

Furthermore, if we consider the interval $1 \leq w \leq 2$, then $-1 \leq w - 2 \leq 0$, and if we set $y = w - 2$ in (32), then $G(w - 2) = \frac{1}{2}V_0$. Substitution of this relation into (36) results in

$$F(w) = \frac{1}{2}V_0 - D_*(w - 1), \quad 1 \leq w \leq 2. \tag{37}$$

Thus by (33) and (37),

$$F(w) = \begin{cases} \frac{1}{2}V_0, & 0 \leq w \leq 1, \\ \frac{1}{2}V_0 - D_*(w - 1), & 1 \leq w \leq 2. \end{cases} \tag{38}$$

If $w \to w + 2$ in (36), or equivalently if $\tau = w + 1$ in (35), then

$$G(w) = F(w + 2) - D_*(w + 1), \quad w \geq -1. \tag{39}$$

Since $G \in [-1, \infty)$, we note that relation (39) allows us to completely determine G in terms of F and D_*. Finally, if $w = \tau + y$ in (39), then

$$G(\tau + y) = F(\tau + y + 2) - D_*(\tau + y + 1). \tag{40}$$

On substituting (40) into (26), we eliminate G, and the non-dimensional stress in the flyer becomes

$$\sigma_*(y, \tau) = F(\tau - y) - F(\tau + y + 2) - D_*(\tau + y + 1) + D_*(\tau). \tag{41}$$

Similarly, the non-dimensional velocity (27) in the flyer becomes

$$v_*(y, \tau) = F(\tau - y) + F(\tau + y + 2) + D_*(\tau + y + 1), \quad \text{for } (y, \tau) \in [-1, 0] \times [0, \infty). \tag{42}$$

With these equations, we are in a position to derive the impact boundary condition for a finite piezoelectric flyer impacting a finite piezoelectric target.

We begin by considering the behavior at the impact face by letting $y = 0$ in (41) and (42):

$$\sigma_*(0, \tau) = F(\tau) - F(\tau + 2) - D_*(\tau + 1) + D_*(\tau), \tag{43}$$

and

$$v_*(0, \tau) = F(\tau) + F(\tau + 2) + D_*(\tau + 1). \tag{44}$$

Now add (43) and (44) to obtain

$$v_*(0, \tau) + \sigma_*(0, \tau) - D_*(\tau) = 2F(\tau), \quad \tau \geq 0. \tag{45}$$

Also, if we subtract (43) from (44), we obtain

$$v_*(0, \tau) - \sigma_*(0, \tau) = 2F(\tau + 2) + 2D_*(\tau + 1) - D_*(\tau), \quad \tau \geq 0. \tag{46}$$

On setting $\tau \to \tau - 2$ in (46) and solving for $2F(\tau)$, we obtain

$$2F(\tau) = v_*(0, \tau - 2) - \sigma_*(0, \tau - 2) + D_*(\tau - 2) - 2D_*(\tau - 1), \quad \tau \geq 2. \tag{47}$$

Then from (38),(45), and (47), we obtain

$$v_*(0,\tau)+\sigma_*(0,\tau)-D_*(\tau)=\begin{cases} V_0, & 0\le\tau\le 1,\\ V_0-2D_*(\tau-1), & 1\le\tau\le 2,\\ v_*(0,\tau-2)-\sigma_*(0,\tau-2) & \\ \quad +D_*(\tau-2)-2D_*(\tau-1), & \tau\ge 2.\end{cases} \tag{48}$$

On substitution of $(21)_2$ and (25) into (48), we obtain the dimensional form of the impact boundary condition:

$$v_0(0,t)+\frac{\sigma_0(0,t)}{z_0}-\frac{h_0}{z_0}D_0(t)=\begin{cases} V_0, & 0\le t\le t_*,\\ V_0-2\frac{h_0}{z_0}D_0(t-t_*), & t_*\le t\le 2t_*,\\ v_0(0,t-2t_*)-\frac{\sigma_0(0,t-2t_*)}{z_0} & \\ \quad +\frac{h_0}{z_0}D_0(t-2t_*)-2\frac{h_0}{z_0}D_0(t-t_*), & t\ge 2t_*.\end{cases} \tag{49}$$

5 Additional boundary and electrical conditions

In addition to the stress-free boundary condition (17) on the back face of the finite flyer, four additional relationships are presented, in this section, for determining the five unknown functions F_0, G_0, F_1, G_1, and D_1, in terms of the field variables of velocity $v_1(x,t)$, stress $\sigma_1(x,t)$, and electric displacement $D_1(t)$ in the piezoelectric target. These relationships are: (1) continuity of stress at the impact face, (2) the impact boundary condition on the target, (3) the continuity condition between the target and semi-infinite elastic half-space, and (4) the integral form of Maxwell's first equation of electrostatics applied to the short circuit assumed to exist between the back faces of the flyer and target, respectively (see Fig. 1).

5.1 Impact boundary condition on the target

Since velocity, stress, and electric displacement are continuous across the impact face $x=0$ during the time[2] that the piezoelectric flyer and target are in contact, we must have that

$$v_0(0,t)=v_1(0,t)\quad\text{and}\quad\sigma_0(0,t)=\sigma_1(0,t)\quad\text{and}\quad D_0(t)=D_1(t),\quad t>0. \tag{50}$$

Here, we do not assume that the velocity, stress, and electric displacement of the flyer and target coincide at $t=0$. For example, $v_0(0,0)=V_0$ by (16), whereas the target is assumed to be initially at rest at $t=0$, i.e., $v_1(0,0)=0$, so $v_0(0,0)\neq v_1(0,0)$, and thus, a shock is formed at the flyer–target boundary $(x,t)=(0,0)$, cf. section 8.1.2 of [4]. Recall that the initial conditions for the target are

$$v_1(x,0)=0,\quad\text{and}\quad\sigma_1(x,0)=D_1(0)=0\quad\text{for}\quad 0\le x\le l. \tag{51}$$

We obtain the impact boundary condition for a piezoelectric target by substituting the continuity conditions (50) into Eq. (49) to arrive at

$$v_1(0,t)+\frac{\sigma_1(0,t)}{z_0}-\frac{h_0}{z_0}D_1(t)=\begin{cases} V_0, & 0<t\le t_*,\\ V_0-2\frac{h_0}{z_0}D_1(t-t_*), & t_*\le t\le 2t_*,\\ v_1(0,t-2t_*)-\frac{\sigma_1(0,t-2t_*)}{z_0} & \\ \quad +\frac{h_0}{z_0}D_1(t-2t_*)-2\frac{h_0}{z_0}D_1(t-t_*), & t\ge 2t_*.\end{cases} \tag{52}$$

Here we note that the stress $\sigma_1(0,t)$, particle velocity $v_1(0,t)$ and electrical displacement $D_1(t)$ at the impact face are unknown quantities, and it is the relationship between them (52) that determines the boundary condition corresponding to impact.

[2] The contact time is infinite since it is assumed that the flyer and target adhere on impact; this assumption is in fact unnecessary in those cases where flyer–target separation does not occur.

5.2 Back face boundary condition on the target

In this section, we simply state the continuity condition between the back face of the target that is bonded to the semi-infinite elastic half-space:

$$\sigma_1(l,t) = z_2 v_1(l,t), \quad t \in \mathbb{R}; \tag{53}$$

the full derivation can be found in [10].

5.3 Electrical boundary condition on the flyer–target

In this section, we show that the time-varying electric potential $V(t)$ is a function of particle displacement and electric displacement during impact for the flyer and target arrangement shown in Fig. 1. The electric potential is given by

$$V(t) = 0 = -\int_{-k}^{0} \mathscr{E}_0(x,t)\mathrm{d}x \; - \int_{0}^{l} \mathscr{E}_1(x,t)\mathrm{d}x. \tag{54}$$

Unlike the gravitational field and other field potentials, the minus sign is used here since the electric field is "governed by Coulomb's law where elements of like sign repel," cf. p. 22 of Sternberg and Smith [28]. On substituting (2) into (54) and specializing this to a short-circuit solution, where the electrical impedance between the back face of the flyer and target is negligible (see Fig. 1), we obtain

$$V(t) = -h_0\,[u_0(0,t) - u_0(-k,t)] + kD_0(t)/\varepsilon_0 - h_1\,[u_1(l,t) - u_1(0,t)] + lD_1(t)/\varepsilon_1 = 0. \tag{55}$$

Here, the quantities in brackets, $u_0(0,t) - u_0(-k,t)$ and $u_1(l,t) - u_1(0,t)$, represent the relative motion of the flyer and target surfaces, respectively;[3] displacement continuity at the impact face $x = 0$ requires that $u_0(0,t) = u_1(0,t)$.

6 Laplace transform of the d'Alembert solution

Solutions for the *true* impact problem with appropriate impact boundary conditions for a finite piezoelectric flyer are obtained in this section by Laplace transform techniques. The derivation of these solutions requires the Laplace transform of the field equations, which is considered here. Let f denote a real-valued, piecewise-continuous function with the property $f(t) = 0, \quad t < 0$. We employ the right-sided or unilateral Laplace transform $\mathscr{L}$ of f defined as

$$\overline{f}(s) = \mathscr{L}\{f\}(s) = \mathscr{L}_t\{f(t)\}(s) \equiv \int_0^\infty f(t)\,e^{-st}\mathrm{d}t. \tag{56}$$

Here $s = \sigma + \mathrm{i}\,\omega$ is generally a complex number with $\mathrm{Re}(s) > 0$, and the overbar on f indicates that the function is in the Laplace transform domain. The Laplace transform of field variables such as $u_1(x,t)$, $\sigma_1(x,t)$ and $v_1(x,t)$ are taken with respect to the time variable t, for example,

$$\overline{\sigma}_1(x,s) = \mathscr{L}_t\{\sigma_1(x,t)\}(s) = \int_0^\infty \sigma_1(x,t)\,e^{-st}\mathrm{d}t. \tag{57}$$

Applying Laplace's shifting theorem to generic d'Alembert functions we see that

$$\mathscr{L}_t\{F(t - x/c)\} = e^{\frac{-sx}{c}}\overline{F}(s), \qquad \mathscr{L}_t\{G(t + x/c)\} = e^{\frac{sx}{c}}\overline{G}(s). \tag{58}$$

[3] Similar behavior is observed in thickness-mode piezoelectric transducers excited by pulse voltage sources for ultrasonic applications [29].

On Laplace transformation of (11), (12), and (13), and use of (58), we obtain Laplace-domain expressions for the displacement, stress, and particle velocity in the target in terms of the transforms of the d'Alembert functions:

$$\overline{u}_1(x,s) = \frac{1}{s}\left[e^{\frac{-sx}{c_1}}\overline{F}_1(s) + e^{\frac{sx}{c_1}}\overline{G}_1(s)\right], \tag{59}$$

$$\overline{\sigma}_1(x,s) = z_1\left[e^{\frac{-sx}{c_1}}\overline{F}_1(s) - e^{\frac{sx}{c_1}}\overline{G}_1(s)\right] + h_1\overline{D}_1(s), \tag{60}$$

$$\overline{v}_1(x,s) = e^{\frac{-sx}{c_1}}\overline{F}_1(s) + e^{\frac{sx}{c_1}}\overline{G}_1(s). \tag{61}$$

Similar equations hold for the flyer:

$$\overline{u}_0(x,s) = \frac{1}{s}\left[e^{\frac{-sx}{c_0}}\overline{F}_0(s) + e^{\frac{sx}{c_0}}\overline{G}_0(s)\right], \tag{62}$$

$$\overline{\sigma}_0(x,s) = z_0\left[e^{\frac{-sx}{c_0}}\overline{F}_0(s) - e^{\frac{sx}{c_0}}\overline{G}_0(s)\right] + h_0\overline{D}_0(s), \tag{63}$$

$$\overline{v}_0(x,s) = e^{\frac{-sx}{c_0}}\overline{F}_0(s) + e^{\frac{sx}{c_0}}\overline{G}_0(s). \tag{64}$$

6.1 Laplace transform of the boundary and potential field conditions

In this section, we present the five equations that are necessary for determination of the five unknown functions $F_0, G_0, F_1, G_1,$ and D_1 used to construct solutions for the stress and velocity in the flyer and target for all time. The five expressions are presented in the Laplace transform domain which is a useful transformation that converts time derivatives into algebraic functions of s. Therefore, we have the following five conditions in the Laplace transform domain:

1. The stress-free boundary condition (17) on the back face of the flyer:

$$\overline{\sigma}_0(-k,s) = 0. \tag{65}$$

2. The stress continuity condition $(50)_2$:

$$\overline{\sigma}_0(0,s) = \overline{\sigma}_1(0,s). \tag{66}$$

3. The impact boundary condition (52):

$$\overline{v}_1(0,s) + \frac{\overline{\sigma}_1(0,s)}{z_0} - \frac{h_0}{z_0}\overline{D}_1(s) = V_0\int_0^{2t_*} e^{-st}\,\mathrm{d}t - \frac{2h_0}{z_0}\int_{t_*}^{\infty} D_1\left(t-t_*\right)e^{-st}\,\mathrm{d}t$$
$$+\int_{2t_*}^{\infty}\left(v_1\left(0,t-2t_*\right) - \frac{\sigma_1\left(0,t-2t_*\right)}{z_0} + \frac{2h_0}{z_0}D_1\left(t-2t_*\right)\right)e^{-st}\,\mathrm{d}t,$$

or

$$\left(\overline{\sigma}_1(0,s) - h_0\overline{D}_1(s)\right)\left(1+e^{-2st_*}\right) + z_0\left(\overline{v}_1(0,s) - \frac{V_0}{s}\right)\left(1-e^{-2st_*}\right) + 2h_0\overline{D}_1(s)e^{-st_*} = 0. \tag{67}$$

For a finite *elastic* flyer, $D_0(t) = 0$ in (49), so that $D_1(t) = 0$ in (52), which implies that (67) specializes to

$$\overline{\sigma}_1(0,s)\left(1+e^{-2st_*}\right) + z_0\left(\overline{v}_1(0,s) - \frac{V_0}{s}\right)\left(1-e^{-2st_*}\right) = 0. \tag{68}$$

For a *semi-infinite elastic* flyer, the travel time in the flyer approaches infinity, $t_* \to \infty$, and (68) further specializes to

$$\overline{\sigma}_1(0,s) + z_0\left(\overline{v}_1(0,s) - \frac{V_0}{s}\right) = 0. \tag{69}$$

Table 1 Elastic, dielectric, and piezoelectric properties of flyer, target, and half-space

Constant	Quartz [30]	PZT-4 [22]	Half-space
C^E (GPa)	86.736	115.41	–
$z = \rho\, c$ (kg m^{-2}/s)	2651×5744.68	7500×4533.38	2651×5744.68
ε_0 (F/m)	$8.854187817 \times 10^{-12}$	$8.854187817 \times 10^{-12}$	–
ε_r	4.40	663.2	–
$\varepsilon = \varepsilon_0\, \varepsilon_r$ (F/m)	3.89584×10^{-11}	$5.87209736 \times 10^{-9}$	–
e (C/m^2)	0.171	15.08	–
$h = e/\varepsilon$ (V/m)	4.38929×10^9	2.5680773×10^9	–
$C^D = C^E + e\, h$ (GPa)	87.487	154.136	–
Flyer/target dimensions (mm)	$k = 10$	$l = 5$	∞

The time-domain form of this impact boundary condition for a semi-infinite elastic flyer was derived in [10] and used (without proof) in [11] for the case of a semi-infinite elastic flyer impacting a finite piezoelectric target.

4. The back face continuity condition (53):

$$\overline{\sigma}_1(l, s) = z_h \overline{v}_1(l, s). \tag{70}$$

5. Maxwell's first equation of electrostatics applied to the short-circuit equation (55) involving the flyer and target:

$$-h_0[\overline{u}_0(0, s) - \overline{u}_0(-k, s)] + \frac{k}{\varepsilon_0}\overline{D}_0(s) - h_1[\overline{u}_1(l, s) - \overline{u}_1(0, s)] + \frac{l}{\varepsilon_1}\overline{D}_1(s) = 0. \tag{71}$$

On substituting Eqs. (59) through (64) into Eqs. (65)–(67) and (70)–(71), and letting $\overline{D}_0(s) = \overline{D}_1(s)$ and $\overline{u}_0(s) = \overline{u}_1(s)$, we obtain algebraic expressions for $\overline{F}_0(s)$, $\overline{G}_0(s)$, $\overline{F}_1(s)$, $\overline{G}_1(s)$, and $\overline{D}_1(s)$. Resubstitution of these algebraic expressions into Eqs. (59) through (64) allows determination of the stress, velocity, and displacement in both the flyer and target in the Laplace transform domain. The algebraic expressions for $\overline{F}_1(s)$, $\overline{G}_1(s)$, and $\overline{D}_1(s)$ appear "Appendix 1"; these expressions will be inverted to the time domain in the next section.

7 Numerical results

The elastic and piezoelectric properties [22,30] of the quartz flyer and PZT-4 target are given in Table 1. The elastic properties for the quartz flyer and half-space are assumed to be identical $z_0 = z_h$.

Solutions in the time domain are illustrated in Figs. 2, 3, and 4 and are found by numerical inversion of the Laplace transform domain expressions using the DAC algorithm [14,15], as modified by Laverty and Gazonas [17] to mitigate the effects of Gibbs' phenomenon. This is accomplished using the so-called Lanczos σ-factors with 2048 terms in the Fourier series and a tolerance equal to 10^{-5}. Laplace transform domain solutions for the stress and particle velocity in the target can be determined through substitution of expressions for $\overline{F}_1(s)$, $\overline{G}_1(s)$, and $\overline{D}_1(s)$ found in "Appendix 1" into Eqs. (60) and (61).

A Mathematica [23] code for the numerical inversion of functions with jump discontinuities using the modified DAC algorithm appears in "Appendix 2." The stress in the target in the Laplace transform domain s is given by the function containing the exponentials in Eq. (82). This same code works equally well for continuous functions, and users need only to replace the last expression $\overline{\sigma}_1(x, s)$ in algorithm (81) with their own Laplace-domain expression, as well as listing the constants appearing in their expression at the beginning of the **Module** command. Mathematica code (81) computes the numerical ILT of the function **Stress** and stores these values in the function Σ. The Mathematica compile function executes this code in less than 8 s on a Dell laptop with a 64-bit OS and 8 GB of RAM running on an Intel(R) Core(TM) i5 CPU, M 560 at 2.67 GHz. The same code executes in 135 s using uncompiled Mathematica code. Mathematica code (86) plots the stress Σ at the center of the piezoelectric target (see Fig. 5); Fig. 5 also compares solutions to the piezoelectric impact problem using a FDTD method, and the commercial finite element code, COMSOL multiphysics [22], both of which exhibit wave dispersion effects.

The impact event that occurs at $t = 0$ induces jump discontinuities in the stress and velocity at the flyer/target impact face. These jump discontinuities appear as step functions that travel into the target and flyer

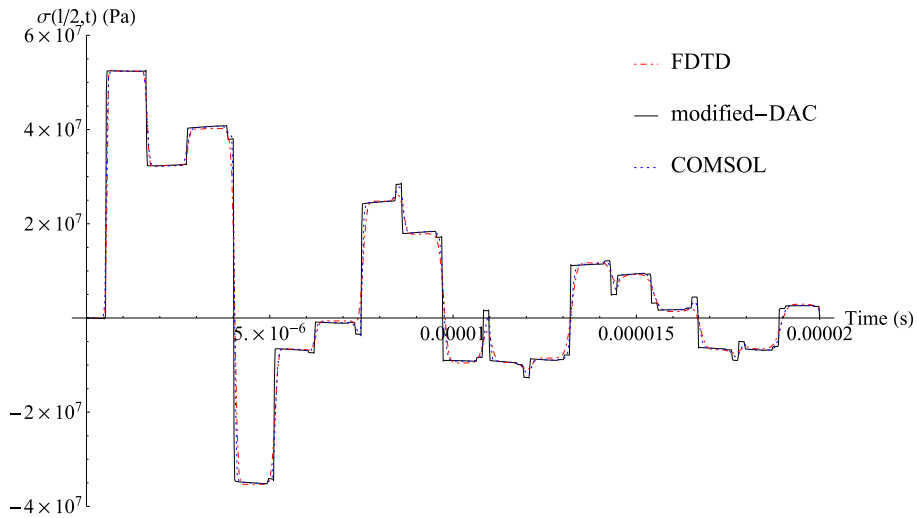

Fig. 2 Stress history at the center of a 5-mm-thick PZT-4 target backed by a semi-infinite elastic half-space under impact by a finite 10-mm-thick quartz flyer with initial velocity $V_0 = 5$ m/s, using material parameters from Table 1

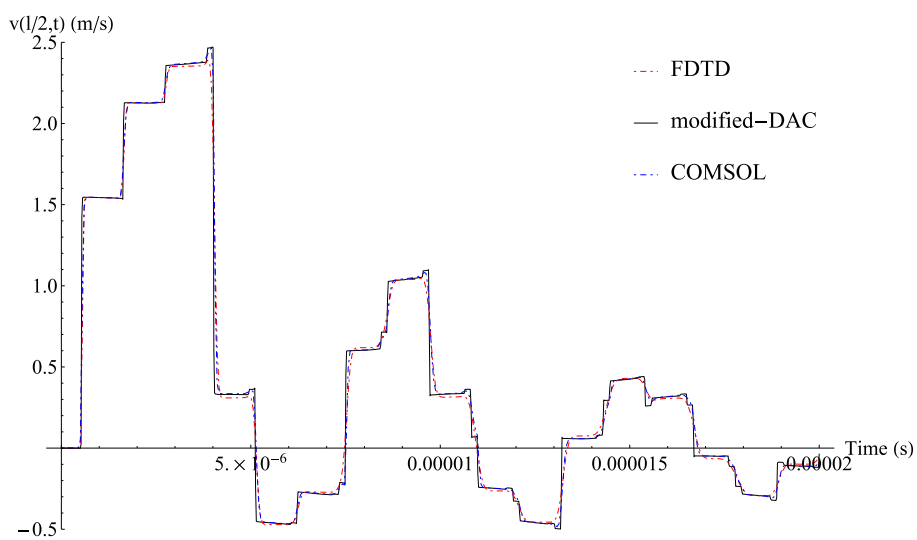

Fig. 3 Velocity history at the center of a 5-mm-thick PZT-4 target backed by a semi-infinite elastic half-space under impact by a finite 10-mm-thick quartz flyer with initial velocity $V_0 = 5$ m/s, using material parameters from Table 1

and are multiply-reflected/transmitted due to the impedance mismatch that exists between the flyer/target and target/half-space interfaces. These wave reflections diminish in amplitude with time as the impact-induced waves are transmitted into the semi-infinite elastic half-space. Finally, the pre-tensile wave that appears clearly in Fig. 5 is due to the synthetic (artificial) material properties that were chosen in this example so as to accentuate the differences between FDTD, COMSOL, and numerical simulations. A pre-tensile "wave" also exists in Fig. 2, but is not perceptible due to the large magnitude in the vertical scale in this figure.

7.1 FDTD and COMSOL numerics

The finite-difference implementation of the problem proceeds using an auxiliary field approach so that (8) is split into two coupled, first-order differential equations. Next, the result of (55) is used to include the electrically induced stress as boundary terms. A central difference approximation of the spatial derivatives and a backward Euler approximation of the temporal derivatives were then used to discretize the problem. As the

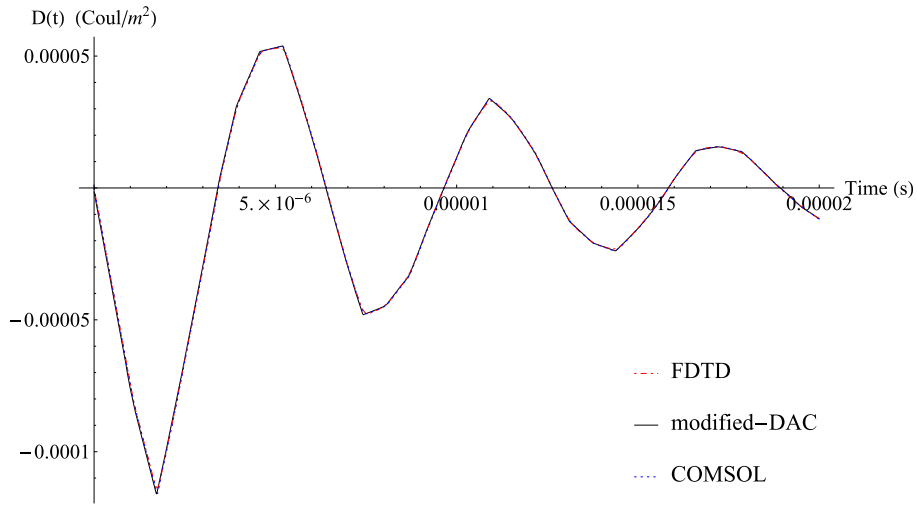

Fig. 4 Displacement current time history at the center of a 5-mm-thick PZT-4 target backed by a semi-infinite elastic half-space under impact by a finite 10-mm-thick quartz flyer with initial velocity $V_0 = 5$ m/s, using material parameters from Table 1

implementation is an implicit method, a sparse matrix is formed describing the spatial derivative approximations and the appropriate boundary conditions are inserted into the matrix. The results in the following plots were computed using a time step sizes of 1 ns and a spatial grid size of 25 μm.

Similarly, an FE model was implemented using the coupled 1-D weak-form partial differential equation (PDE) interfaces in the COMSOL multiphysics software. The governing equations used were Gauss's law and the wave equation, given by Eqs. (7) and (8). However, the constitutive relations were given by the stress-charge form of the piezoelectric constitutive relations (see Eq. B-5 of [31]) with the resultant change in the definition for the wave speed, c, and the piezoelectric coupling coefficient. The impactor, target and semi-infinite elastic half-space were each described by their own set of coupled PDE's. Matching boundary conditions were then used to enforce continuity between these components. An artificial damping weak term was added to remove spurious high-frequency response. Results using both linear and quadratic Lagrange shape functions were obtained. Time stepping was done with a generalized alpha scheme with the maximum time step limited to 1 ns. The mesh density was 50 μm. Results obtained using quadratic shape functions are presented in Figs. 2, 3 and 4.

8 Discussion and conclusions

Numerical solutions for stress, particle velocity, and electrical displacement in a lead zirconate titanate (PZT-4) target, backed by an elastic half-space and under impact by a one-dimensional finite quartz flyer, compare well with the numerical solutions obtained using a finite-difference time-domain (FDTD) code and the commercial finite element code, COMSOL multiphysics [22] (see Figs. 2, 3, 4, 5). The numerical FDTD code and the COMSOL simulations corroborate the derived numerical inverse Laplace transform solutions using a modified DAC algorithm listed in "Appendix 2." We are not aware of any other general elastodynamic flyer–target impact solutions in the literature, where both the flyer and the target are composed of different piezoelectric materials, are of arbitrary length, and treat the occurrence of multiply-reflected impact-induced waves. In "Appendix 3," we compute the relative error between our numerical ILT-derived solution and the exact analytical solution derived by Le [12,13] for the special case of a finite-length piezoceramic rod, traveling at an initial constant velocity, that impacts a second, identical, but stationary piezoceramic rod; it is shown that the numerical ILT solutions are quite accurate over the two-way travel time or impact interval $0 \leq t \leq 2l/c$.

The numerical solutions for a finite-thickness piezoelectric flyer impacting a finite-thickness piezoelectric target composed of synthetic elastic and piezoelectric properties reveal the nearly instantaneous appearance of a tensile stress wave at the center of the target. The tensile stress increases linearly in amplitude (see Fig. 5) and is formed by the $\mathscr{E}$-field-induced polarization of the material in the initially unstressed region of the target. This behavior is similar to that observed for a semi-infinite elastic flyer that collides with a finite PZT-4 target

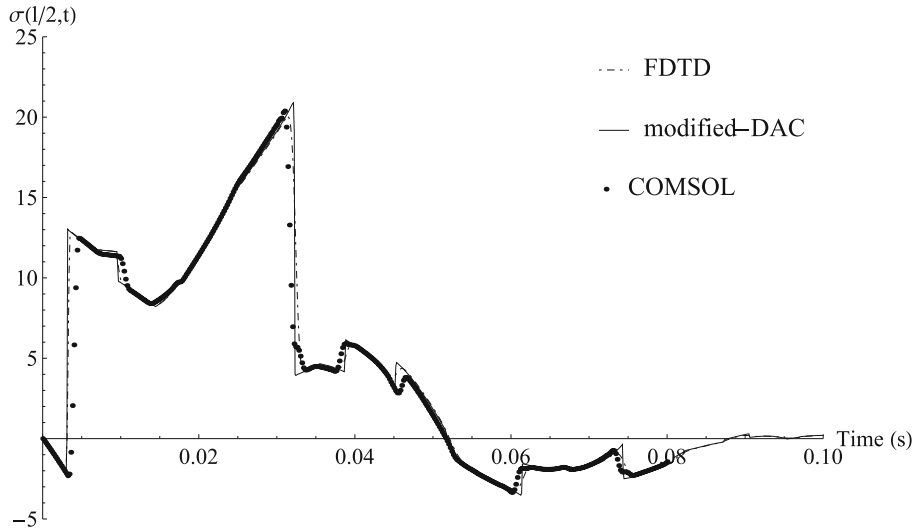

Fig. 5 Stress time history at the center of a 5-mm-thick piezoelectric target backed by a semi-infinite elastic half-space under impact by a 10-mm-thick piezoelectric flyer with initial velocity $V_0 = 5$ m/s; synthetic elastic and piezoelectric material parameters from code (81) (see Table 2) are used to illustrate the differences between the FDTD, ILT, and COMSOL numerical solution methods

Table 2 Synthetic elastic, dielectric, and piezoelectric properties of flyer, target, and half-space

Constant	Flyer	Target	**Half-space**
C^E (GPa)	2	3	–
$z = \rho\, c$ (kg m^{-2}/s)	8×0.687	9×0.733	8×0.687
ε_0 (F/m)	1.5	1.5	–
ε_r	6	7	–
$\varepsilon = \varepsilon_0\, \varepsilon_r$ (F/m)	9	10.5	–
e (C/m^2)	4	5	–
$h = e/\varepsilon$ (V/m)	0.444	0.476	–
$C^D = C^E + e\, h$ (GPa)	3.778	5.381	–
Flyer/target dimensions (mm)	$k = 10$	$l = 5$	∞

studied in [11]; the magnitude of this effect is negligible in the "quartz on PZT-4" impact solution illustrated in Fig. 2.

For *nonlinear* piezoelectric media, Chen et al. [1] report that this wave cannot be a shock wave but must be an acceleration wave since the wave speed depends upon a time-dependent displacement current $D(t)$ (see Chen et al. [1] equation (4.12)). The nearly instantaneous appearance of the stress wave occurs since the speed of light is about five orders of magnitude greater than the longitudinal wave speed in the target. The tensile stress wave is eventually overcome by the impact-induced compressive stress wave at about 1.25 ms, cf. Fig. 5.

Finally, we have shown that the new impact boundary condition (52) for a finite piezoelectric flyer includes as a special case the impact boundary condition for an elastic flyer of finite extent or an elastic flyer of semi-infinite extent [10,11].

Acknowledgments The authors wish to thank reviewer 1 for identifying the closed-form solutions found in the Le [12,13] references that were used to verify the ILT numerical solutions appearing in "Appendix 3."

Appendix 1: Laplace transform domain functions $\overline{F}_1(s)$, $\overline{G}_1(s)$, and $\overline{D}_1(s)$

Appendix 1 lists the Laplace transform domain functions $\overline{F}_1(s)$, $\overline{G}_1(s)$, and $\overline{D}_1(s)$ that are substituted into (60) for the Laplace transform domain stress $\overline{\sigma}_1(x, s)$ in the target that is inverted to the time-domain using the Mathematica algorithm in "Appendix 2."

$$\overline{F}_1(s) = \frac{\overline{n}_{F_1}(s)}{\overline{d}_{F_1}(s)}, \tag{72}$$

where

$$\begin{aligned}
\overline{n}_{F_1}(s) = {} & V_0 z_0 e^{-\frac{ks}{c_0}} \left(e^{\frac{ks}{c_0}} - 1\right) \Big(e^{\frac{ks}{c_0}+\frac{ls}{c_1}} (\varepsilon_1(\varepsilon_0(-2h_0^2(z_1+z_2) + h_1 h_0(z_1+z_2) - h_1^2 z_0\Big) \\
& + ksz_0(z_1+z_2)) + lsz_0(z_1+z_2)\varepsilon_0) + e^{\frac{ls}{c_1}} (\varepsilon_1(ksz_0(z_1+z_2) - \varepsilon_0(-2h_0^2(z_1+z_2) \\
& + h_1 h_0(z_1+z_2) + h_1^2 z_0)) + lsz_0(z_1+z_2)\varepsilon_0) + h_1\varepsilon_0\varepsilon_1(h_1 z_0 - h_0 z_1) e^{\frac{ks}{c_0}} \\
& + h_1\varepsilon_0\varepsilon_1(h_1 z_0 + h_0 z_1)),
\end{aligned} \tag{73}$$

$$\begin{aligned}
\overline{d}_{F_1}(s) = {} & 4s(\sinh\left(\frac{ks}{c_0}\right) \left(\sinh\left(\frac{ls}{c_1}\right) (\varepsilon_1(ksz_0^2 z_2 - \varepsilon_0(h_1^2 z_0^2 + h_0^2 z_1^2)\right) + lsz_2 z_0^2 \varepsilon_0) \\
& + z_1 \cosh\left(\frac{ls}{c_1}\right) (h_0^2(-z_2)\varepsilon_0\varepsilon_1 + ksz_0^2\varepsilon_1 + lsz_0^2\varepsilon_0)) \\
& + z_0 \cosh\left(\frac{ks}{c_0}\right) \left(\sinh\left(\frac{ls}{c_1}\right) (\varepsilon_1(ksz_1^2 - (2h_0^2 - 2h_1 h_0 + h_1^2) z_2\varepsilon_0) + lsz_1^2\varepsilon_0\right) \\
& + z_1 \cosh\left(\frac{ls}{c_1}\right) (\varepsilon_1(ksz_2 - 2(h_0^2 - h_1 h_0 + h_1^2)\varepsilon_0) + lsz_2\varepsilon_0) + 2h_1(h_1 - h_0) z_1 \varepsilon_0 \varepsilon_1) \\
& + 2h_0 z_0 \varepsilon_0 \varepsilon_1 \left((h_0 - h_1)\left(z_2 \sinh\left(\frac{ls}{c_1}\right) + z_1 \cosh\left(\frac{ls}{c_1}\right)\right) + h_1 z_1\right)\Big).
\end{aligned} \tag{74}$$

$$\overline{G}_1(s) = \frac{\overline{n}_{G_1}(s)}{\overline{d}_{G_1}(s)}, \tag{75}$$

where

$$\begin{aligned}
\overline{n}_{G_1}(s) = {} & V_0 z_0 \left(e^{\frac{ks}{c_0}} - 1\right) e^{-\frac{ks}{c_0}-\frac{ls}{c_1}} (\varepsilon_1(ksz_0(z_1 - z_2)\left(e^{\frac{ks}{c_0}} + 1\right) \\
& - \varepsilon_0(h_1 h_0 \left(e^{\frac{ks}{c_0}} - 1\right)(z_1\left(e^{\frac{ls}{c_1}} - 1) + z_2\right) + h_1^2 z_0 \left(e^{\frac{ks}{c_0}} + 1\right)\left(e^{\frac{ls}{c_1}} - 1\right) \\
& + 2h_0^2(z_1 - z_2)\left(e^{\frac{ks}{c_0}} - 1\right)\Big)\Big) + lsz_0(z_1 - z_2)\varepsilon_0 \left(e^{\frac{ks}{c_0}} + 1)\right),
\end{aligned} \tag{76}$$

$$\begin{aligned}
\overline{d}_{G_1}(s) = {} & V_0 z_0 \left(e^{\frac{ks}{c_0}} - 1\right) e^{-\frac{ks}{c_0}-\frac{ls}{c_1}} (\varepsilon_1(ksz_0(z_1 - z_2)(e^{\frac{ks}{c_0}} + 1) \\
& - \varepsilon_0(h_1 h_0 \left(e^{\frac{ks}{c_0}} - 1\right)(z_1\left(e^{\frac{ls}{c_1}} - 1) + z_2\right) + h_1^2 z_0 \left(e^{\frac{ks}{c_0}} + 1\right)(e^{\frac{ls}{c_1}} - 1) \\
& + 2h_0^2(z_1 - z_2)\left(e^{\frac{ks}{c_0}} - 1\right)\Big)\Big) + lsz_0(z_1 - z_2)\varepsilon_0 \left(e^{\frac{ks}{c_0}} + 1)\right)\Big).
\end{aligned} \tag{77}$$

$$\overline{D}_1(s) = \frac{\overline{n}_{D_1}(s)}{\overline{d}_{D_1}(s)}, \tag{78}$$

where

$$\begin{aligned}
\overline{n}_{D_1}(s) = {} & V_0 z_0 \varepsilon_0 \varepsilon_1 \left(e^{\frac{ks}{c_0}} - 1\right)\left(-e^{-\frac{ks}{c_0}-\frac{ls}{c_1}}\right)\left(h_1 z_0 \left(e^{\frac{ks}{c_0}} + 1\right)\left(e^{\frac{ls}{c_1}} - 1\right)\left((z_1 + z_2)e^{\frac{ls}{c_1}} - z_1 + z_2\right)\right. \\
& \left. + h_0 z_1 \left(e^{\frac{ks}{c_0}} - 1\right)\left((z_1 + z_2)e^{\frac{2ls}{c_1}} - z_1 + z_2\right)\right),
\end{aligned} \tag{79}$$

$$\overline{d}_{D_1}(s) = 4s\left(\sinh\left(\frac{ks}{c_0}\right)\left(\sinh\left(\frac{ls}{c_1}\right)\left(\varepsilon_1\left(ksz_0^2 z_2 - \varepsilon_0\left(h_1^2 z_0^2 + h_0^2 z_1^2\right)\right) + lsz_2 z_0^2 \varepsilon_0\right)\right.\right.$$

$$
\begin{aligned}
&+ z_1 \cosh\left(\frac{ls}{c_1}\right)\left(h_0^2(-z_2)\varepsilon_0\varepsilon_1 + ksz_0^2\varepsilon_1 + lsz_0^2\varepsilon_0\right)\Big) \\
&+ z_0 \cosh\left(\frac{ks}{c_0}\right)\Big(\sinh\left(\frac{ls}{c_1}\right)\left(\varepsilon_1\left(ksz_1^2 - \left(2h_0^2 - 2h_1h_0 + h_1^2\right)z_2\varepsilon_0\right) + lsz_1^2\varepsilon_0\right) \\
&+ z_1 \cosh\left(\frac{ls}{c_1}\right)\left(\varepsilon_1\left(ksz_2 - 2\left(h_0^2 - h_1h_0 + h_1^2\right)\varepsilon_0\right) + lsz_2\varepsilon_0\right) + 2h_1(h_1 - h_0)z_1\varepsilon_0\varepsilon_1\Big) \\
&+ 2h_0z_0\varepsilon_0\varepsilon_1\left((h_0 - h_1)\left(z_2\sinh\left(\frac{ls}{c_1}\right) + z_1\cosh\left(\frac{ls}{c_1}\right)\right) + h_1z_1\right)\Big).
\end{aligned}
\tag{80}
$$

Appendix 2: Mathematica code for determining the numerical ILT using the modified DAC algorithm [11, 17]

The following Mathematica [23] source code is useful for determining the numerical inverse Laplace transform (ILT) of functions with jump discontinuities using the modified Dubner–Abate–Crump (DAC) algorithm [11, 17]. Figure 5 illustrates the stress time history in the target and use of the ILT algorithm for a set of synthetic flyer and target elastic and piezoelectric properties.

Mathematica code to compile the Laplace transform domain function $\overline{\sigma}_1(x, s)$

$$
\begin{aligned}
&\textbf{Stress} = \textbf{Compile}\Big[\{\{s, _\text{Complex}\}\}, \textbf{Module}\Big[\{l, k, x, \text{eo}, \text{e0}, \text{e1}, \text{Ce0}, \text{Ce1}, \text{ers0}, \text{ers1}, \varepsilon 0, \varepsilon 1, \text{h0}, \text{h1}, \\
&\text{M0}, \text{M1}, \rho\,0, \rho\,1, \text{c0}, \text{c1}, \text{V0}, \text{z0}, \text{z1}, \text{z2}, \text{t0}\}, l = 5\times 10^{-3}; k = 10\times 10^{-3}; x = \frac{l}{2}; \text{eo} = 1.5; \\
&\text{Ce0} = 2; \text{Ce1} = 3; \text{e0} = 4; \text{e1} = 5; \text{ers0} = 6; \text{ers1} = 7; \varepsilon 0 = \text{eo ers0}; \varepsilon 1 = \text{eo ers1}; \\
&\text{h0} = \frac{\text{e0}}{\varepsilon 0}; \text{h1} = \frac{\text{e1}}{\varepsilon 1}; \text{M0} = \text{Ce0} + \text{e0 h0}; \text{M1} = \text{Ce1} + \text{e1 h1}; \rho\,0 = 8; \rho\,1 = 9; \\
&\text{c0} = \sqrt{\frac{\text{M0}}{\rho\,0}}; \text{c1} = \sqrt{\frac{\text{M1}}{\rho\,1}}; \text{V0} = 5; \text{z0} = \rho\,0\ \text{c0}; \text{z1} = \rho\,1\ \text{c1}; \text{z2} = \text{z0}; \overline{\sigma}_1(x, s)\Big]\Big];
\end{aligned}
\tag{81}
$$

$\overline{\sigma}_1(x, s)$ in the above code is given by the following Laplace transform domain expression for the stress in the target

$$
\overline{\sigma}_1(x, s) = \frac{Num(x, s)}{Denom(s)},
\tag{82}
$$

where

$$
\begin{aligned}
Num(x, s) = {} & \text{V0z0}\left(e^{\frac{ks}{\text{c0}}} - 1\right)e^{-\frac{sx}{\text{c1}}}\Big(-\text{z1}e^{\frac{ks}{\text{c0}}+\frac{2sx}{\text{c1}}}\Big(\varepsilon 1\big(\varepsilon 0\big(2\text{h0}^2(\text{z2} - \text{z1}) + \text{h0h1}(\text{z1} - \text{z2}) + \text{h1}^2\text{z0}\big) \\
& + ks\text{z0}(\text{z1} - \text{z2})\big) + ls\text{z0}\varepsilon 0(\text{z1} - \text{z2})\Big) \\
& + \text{z1}e^{\frac{ks}{\text{c0}}+\frac{2ls}{\text{c1}}}\Big(\varepsilon 1\big(\varepsilon 0\big(-2\text{h0}^2(\text{z1} + \text{z2}) + \text{h0h1}(\text{z1} + \text{z2}) - \text{h1}^2\text{z0}\big) \\
& + ks\text{z0}(\text{z1} + \text{z2})\big) + ls\text{z0}\varepsilon 0(\text{z1} + \text{z2})\Big) - \text{h1}\varepsilon 0\varepsilon 1(\text{z1} + \text{z2})(\text{h0z1} + \text{h1z0})e^{\frac{s(\text{c0}(l+x)+\text{c1}k)}{\text{c0c1}}} \\
& + \text{h1z1}\varepsilon 0\varepsilon 1(\text{h0z1} + \text{h1z0})e^{\frac{s(\text{c0}(l+2x)+\text{c1}k)}{\text{c0c1}}} + \text{h1z1}\varepsilon 0\varepsilon 1(\text{h1z0} - \text{h0z1})e^{\frac{ks}{\text{c0}}+\frac{ls}{\text{c1}}} \\
& - \text{h1}\varepsilon 0\varepsilon 1(\text{z1} - \text{z2})(\text{h1z0} - \text{h0z1})e^{\frac{ks}{\text{c0}}+\frac{sx}{\text{c1}}} + 2\text{h1}^2\text{z0z1}\varepsilon 0\varepsilon 1e^{\frac{s(\text{c0}(l+x)+\text{c1}k)}{\text{c0c1}}} \\
& - \text{z1}e^{\frac{2sx}{\text{c1}}}\Big(\varepsilon 1\big(\varepsilon 0\big(2\text{h0}^2(\text{z1} - \text{z2}) + \text{h0h1}(\text{z2} - \text{z1}) + \text{h1}^2\text{z0}\big) + ks\text{z0}(\text{z1} - \text{z2})\big) \\
& + ls\text{z0}\varepsilon 0(\text{z1} - \text{z2})\Big) + \text{z1}e^{\frac{2ls}{\text{c1}}}\Big(\varepsilon 1\,(ks\text{z0}(\text{z1} + \text{z2}) \\
& - \varepsilon 0\left(-2\text{h0}^2(\text{z1} + \text{z2}) + \text{h0h1}(\text{z1} + \text{z2}) + \text{h1}^2\text{z0}\right)\Big)
\end{aligned}
$$

$$
\begin{aligned}
&+ lsz0\varepsilon0(z1+z2)\big) - h1\varepsilon0\varepsilon1(z1+z2)e^{\frac{s(2l+x)}{c1}}(h1z0-h0z1)\\
&+ h1z1\varepsilon0\varepsilon1e^{\frac{s(l+2x)}{c1}}(h1z0-h0z1)\\
&+ h1z1\varepsilon0\varepsilon1e^{\frac{ls}{c1}}(h0z1+h1z0) - h1\varepsilon0\varepsilon1(z1-z2)e^{\frac{sx}{c1}}(h0z1+h1z0) + 2h1^2z0z1\varepsilon0\varepsilon1e^{\frac{s(l+x)}{c1}}\big),
\end{aligned}
\tag{83}
$$

and

$$
\begin{aligned}
Denom(s) = s\Big(&\varepsilon1\big(\varepsilon0\big(-h0^2\big(e^{\frac{ks}{c0}}-1\big)\Big(2z0\big(e^{\frac{ks}{c0}}-1\big)\big(z1\big(e^{\frac{2ls}{c1}}+1\big)+z2\big(e^{\frac{2ls}{c1}}-1\big)\big)\\
&+ z1\big(e^{\frac{ks}{c0}}+1\big)\big(z1\big(e^{\frac{2ls}{c1}}-1\big)+z2\big(e^{\frac{2ls}{c1}}+1\big)\big)\Big)\\
&+2h0h1z0\big(e^{\frac{ks}{c0}}-1\big)^2\big(e^{\frac{ls}{c1}}-1\big)\big(z1\big(e^{\frac{ls}{c1}}-1\big)\\
&+ z2\big(e^{\frac{ls}{c1}}+1\big)\big) - h1^2z0\big(e^{\frac{ls}{c1}}-1\big)\big(z0\big(e^{\frac{2ks}{c0}}-1\big)\big(e^{\frac{ls}{c1}}+1\big)\\
&+\big(e^{\frac{2ks}{c0}}+1\big)\big(2z1\big(e^{\frac{ls}{c1}}-1\big)+z2\big(e^{\frac{ls}{c1}}+1\big)\big)\big)\big)\\
&+ ksz0\big(z0\big(e^{\frac{2ks}{c0}}-1\big)\big(z1\big(e^{\frac{2ls}{c1}}+1\big)+z2\big(e^{\frac{2ls}{c1}}-1\big)\big)\\
&+z1\big(e^{\frac{2ks}{c0}}+1\big)\big(z1\big(e^{\frac{2ls}{c1}}-1\big)+z2\big(e^{\frac{2ls}{c1}}+1\big)\big)\big)\big)\\
&+ lsz0\varepsilon0\big(z0\big(e^{\frac{2ks}{c0}}-1\big)\big(z1\big(e^{\frac{2ls}{c1}}+1\big)+z2\big(e^{\frac{2ls}{c1}}-1\big)\big)\\
&+z1\big(e^{\frac{2ks}{c0}}+1\big)\big(z1\big(e^{\frac{2ls}{c1}}-1\big)+z2\big(e^{\frac{2ls}{c1}}+1\big)\big)\big)\Big).
\end{aligned}
\tag{84}
$$

Mathematica code to perform the ILT of function **Stress** defined in "Mathematica code to compile the Laplace transform domain function $\overline{\sigma}_1(x,s)$"

$$
\begin{aligned}
\Sigma = \mathbf{Compile}\big[\{\},\ &\mathbf{Module}\big[\{\text{sumcp, sumsp, tf, tol}, a, \text{tot, c0}, \tau, \text{dt}, \sigma, \text{arg, coeffs, cospart, c1, c2, sinpart,}\\
&\text{kpd}, t, \text{kpt}\}, \text{tf} = 0.1; \text{tol} = 0.00001; a = -\frac{\mathbf{Log}(\text{tol})}{2.\text{tf}}; \text{tot} = 2048;\\
&\text{c0} = \mathbf{Stress}[a]; \tau = 1000; \text{dt} = \frac{\text{tf}}{\tau};\\
&\mathbf{Table}\big[\text{sumcp} = 0.; \text{sumsp} = 0.; \mathbf{Do}\big[\text{kpd} = \frac{\pi\ k}{\text{tot}}; \text{kpt} = \frac{\pi\ k}{\text{tf}};\\
&\sigma = \frac{\mathbf{Sin}[\text{kpd}]}{\text{kpd}}; \text{coeffs} = \mathbf{Stress}[a + i\ \text{kpt}];\\
&\text{c1} = \mathbf{Re}[\text{coeffs}]; \text{c2} = \mathbf{Im}[\text{coeffs}]; \text{cospart} = \text{c1}\ \sigma\ \mathbf{Cos}[\text{kpt}\ t]; \text{sumcp} = \text{cospart} + \text{sumcp};\\
&\text{sinpart} = \text{c2}\ \sigma\ \mathbf{Sin}(\text{kpt}\ t); \text{sumsp} = \text{sinpart} + \text{sumsp}, \{k, 1, \text{tot}\}\big]; \frac{\mathbf{Exp}(a\ t)\big(\frac{\text{c0}}{2.} + \text{sumcp} - \text{sumsp}\big)}{\text{tf}},\\
&\{t, \text{dt, tf, dt}\}\big]\big], \mathbf{CompilationOptions} \to\\
&\{\text{"InlineExternalDefinitions"} \to \mathbf{True}, \text{"InlineCompiledFunctions"} \to \mathbf{True}\}\big];
\end{aligned}
\tag{85}
$$

Mathematica code to plot the numerical ILT of Σ defined in (85)

$$
\begin{aligned}
&\text{Ce0} = 86.736 \times 10^9; \text{Ce1} = 115.41 \times 10^9; \rho\,0 = 2651; \rho\,1 = 7500;\\
&\text{c0} = \sqrt{\frac{\text{Ce0}}{\rho\,0}}; \text{c1} = \sqrt{\frac{\text{Ce1}}{\rho\,1}}; \text{V0} = 5; \text{z0} = \text{c0}\,\rho\,0; \text{z1} = \text{c1}\,\rho\,1;\\
&\mathbf{ListPlot}\big[\Sigma[\ \ ], \mathbf{Joined} \to \mathbf{True}, \mathbf{BaseStyle} \to \{\mathbf{FontFamily} \to \text{"Times"}, \mathbf{FontSize} \to 14\},\\
&\mathbf{AxesLabel} \to \{\text{"Time (s)"}, \text{"}\sigma(l/2, t)''\}, \mathbf{PlotLabel} \to \text{"Stress"}, \mathbf{DataRange} \to \{0, 0.1\},\\
&\mathbf{PlotRange} \to \{\{0, 0.1\}, \{-10, 25\}\}, \mathbf{PlotStyle} \to \mathbf{Black}\big]
\end{aligned}
\tag{86}
$$

Appendix 3: Verification of the numerical ILT solutions with the closed-form results of Le [12,13]

In this Appendix 3, we determine the relative error between the exact solution for the electric displacement derived by Le [12,13] and the numerical ILT solution using the Mathematica algorithm listed in "Appendix 2." Le [12,13] studies the problem of a finite-length piezoceramic rod, traveling at an initial constant velocity, that impacts a second, identical, but stationary piezoceramic rod; exact solutions for electric displacement and stress are provided, up until the first wave reflection, for the case when the external ends of the rods are electrically short-circuited. For identical piezoceramic rods, the electric displacement can be written as

$$D(t) = \frac{\varepsilon h}{2l}[u(l,t) - u(-l,t)]. \tag{87}$$

Le [12,13] provides closed-form analytical expressions for the relative displacement $u(l,t) - u(-l,t)$ of the rod ends used in Eq. (87) and illustrated in Fig. 6 for the time interval $0 \le t \le 2l/c$. Since the piezoceramic rods

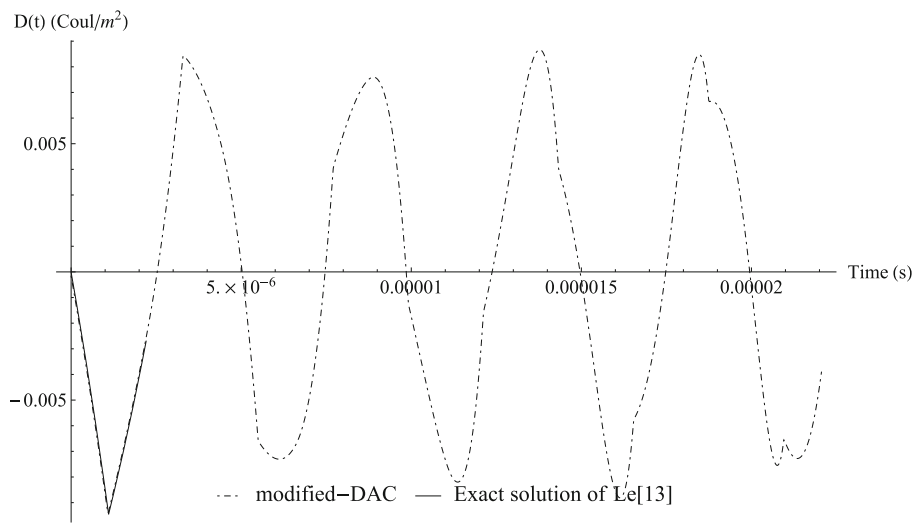

Fig. 6 Comparison of numerical and exact displacement current time histories in a 5-mm-thick PZT-4 target under impact by a 5-mm-thick PZT-4 flyer with initial velocity $V_0 = 5$ m/s, using PZT-4 material parameters from Table 1; the exact solution of Le [13] is plotted for the time interval time $0 \le t \le 2l/c$

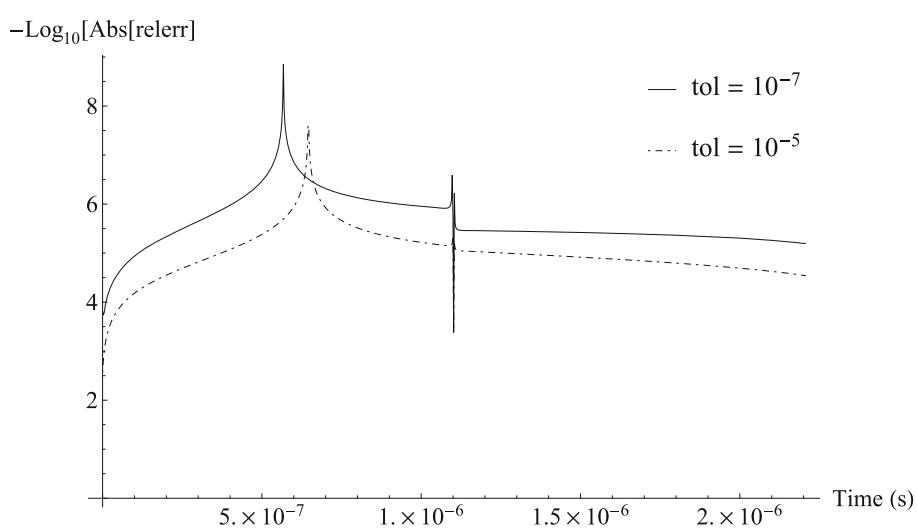

Fig. 7 Numerical accuracy of the modified DAC displacement current solution depicted in Fig. 6 for two tolerance values tol $= 10^{-5}$ and tol $= 10^{-7}$ used in the ILT algorithm [Eq. (85)] over the time interval $0 \le t \le 2l/c$; over this interval, the numerical solution accuracy ranges from about 3 to 9 significant digits

are finite in extent, the electric displacement sinusoidally oscillates in time and does not diminish in amplitude as in the example where the target is backed by a semi-infinite half-space (Fig. 4); the PZT-4 constants used to generate the solutions appearing in Fig. 6 can be found in Table 1.

If $D(t)$ represents the exact value of the electric displacement given by Eq. (87), and $\widetilde{D}(t)$ is the approximate ILT value; then, the relative error, relerr, of $\widetilde{D}(t)$ is given by

$$\text{relerr} = 1 - \frac{\widetilde{D}(t)}{D(t)}. \tag{88}$$

It can be shown that $-\text{Log}_{10}[|\text{relerr}|]$ (see Fig. 7) is a measure of the approximate number of significant digits in the solution. Note that relerr is defined only if $D(t) \neq 0$.

References

1. Chen, P.J., Davison, L., McCarthy, M.F.: Electrical responses of nonlinear piezoelectric materials to plane waves of uniaxial strain. J. Appl. Phys. **47**(11), 4759–4764 (1976)
2. Graham, R.A.: Second and third order piezoelectric stress constants of lithium niobate as determined by the impact loading technique. J. Appl. Phys. **48**(6), 2153–2163 (1977)
3. Wang, X., Dai, H.L.: Dynamic focusing-effect of piezoelectric fibers subjected to radial impact. Compos. Struct. **78**(4), 567–574 (2007)
4. Davison, L.: Fundamentals of Shock Wave Propagation in Solids. Springer, Heidelberg (2008)
5. Redwood, M.: Transient performance of a piezoelectric transducer. J. Acoust. Soc. Am. **33**(4), 527–536 (1961)
6. Steutzer, O.M.: Multiple reflections in a free piezoelectric plate. J. Acoust. Soc. Am. **42**(2), 502–508 (1967)
7. Clayton, J.D.: Modeling nonlinear electromechanical behavior of shocked silicon carbide. J. Appl. Phys. **107** (2010)
8. Graham, R.A.: Strain dependence of longitudinal piezoelectric, elastic, and dielectric constants of x-cut quartz. J. Appl. Phys. **6**(12), 4779–4792 (1972)
9. Lysne, P.C.: One dimensional theory of polarization by shock waves: Application to quartz gauges. J. Appl. Phys. **43**(2), 425–431 (1972)
10. Gazonas, G.A., Scheidler, M.J., Velo, A.P.: Exact analytical solutions for elastodynamic impact (2015) (in review)
11. Gazonas, G.A., Wildman, R.A., Hopkins, D.A.: Elastodynamic impact into piezoelectric media. U.S. Army Research Laboratory, ARL-TR-7056, September (2014)
12. Le, K.C.: On the impact of piezoceramic rods. Mech. Solids **3**, 312–316 (1987)
13. Le, K.C.: Vibrations of Shells and Rods. Springer, Berlin (1999)
14. Dubner, H., Abate, J.: Numerical inversion of Laplace transforms by relating them to the finite Fourier cosine transform. J. ACM **15**(1), 115–123 (1968)
15. Durbin, F.: Numerical inversion of Laplace transforms: an efficient improvement to Dubner and Abate's method. Comput. J. **17**(4), 371–376 (1974)
16. Crump, K.: Numerical inversion of Laplace transforms using a Fourier series approximation. J. ACM **23**(1), 89–96 (1976)
17. Laverty, R., Gazonas, G.A.: An improvement to the Fourier series method for inversion of Laplace transforms applied to elastic and viscoelastic waves. Int. J. Comput. Methods **3**(1), 57–69 (2006)
18. Su, Y., Ma, C.: Transient wave analysis of a cantilever Timoshenko beam subjected to impact loading by Laplace transform and normal mode methods. Int. J. Solids Struct. **49**, 1158–1176 (2012)
19. Ing, Y., Liao, H., Huang, K.: The extended Durbin method and its application for piezoelectric wave propagation problems. Int. J. Solids Struct. **50**, 4000–4009 (2013)
20. Sirwah, M.A.: Sloshing waves in a heated viscoelastic fluid layer in an excited rectangular tank. Phys. Lett. A **378**, 3289–3300 (2014)
21. Randow, C.L., Gazonas, G.A.: Transient stress wave propagation in one-dimensional micropolar bodies. Int. J. Solids Struct. **46**(5), 1218–1228 (2009)
22. COMSOL Multiphysics Reference Manual, version 4.4. Burlington, MA: COMSOL, Inc. (2013)
23. Mathematica Edition: version 9.0. Champaign, IL: Wolfram Research (2013)
24. Cady, W.G.: Piezoelectricity, vol. 1. Dover Publications, New York (1964)
25. Standards on piezoelectric crystals. In: Proceedings of the I.R.E.; New York: The Institute of Radio Engineers, pp. 1378–1395 (1949)
26. Lorrain, P., Corson, D.R.: Electromagnetic Fields and Waves, vol. 2. W.H. Freeman & Co., New York (1970)
27. Costen, R.C., Adamson, D.: Three-dimensional derivation of the electrodynamic jump conditions and momentum-energy laws at a moving boundary. Proc. IEEE **53**(9), 1181–1196 (1965)
28. Sternberg, W.J., Smith, T.L.: The Theory of Potential and Spherical Harmonics. University of Toronto Press, Toronto (1964)
29. Zhang, H.L., Li, M.X., Ying, C.F.: Complete solutions of the transient behavior of a transmitting thickness-mode piezoelectric transducer and their physical interpretations. J. Acoust. Soc. Am. **74**(4), 1105–1114 (1983)
30. Davison, L., Graham, R.: Shock compression of solids. Phys. Rep. Rev. Sect. Phys. Lett. **55**(4), 255–379 (1979)
31. Hopkins, D.A., Gazonas, G.A.: Wave propagation in second-order nonlinear piezoelectric media. U.S. Army Research Laboratory, ARL-TR-5766, September (2011)

1 (PDF) DEFENSE TECH INFO CTR
DTIC OCA

2 (PDF) US ARMY RSRCH LAB
IMAL HRA MAIL & RECORDS MGMT
RDRL CIO LL TECHL LIB

1 (PDF) GOVT PRNTG OFC
A MALHOTRA

63 (PDF) US ARMY RSRCH LAB
RDRL WM
B FORCH
S KARNA
J MCCAULEY
J ZABINSKI
RDRL WML B
I BATYREV
J BRENNAN
E BYRD
W D MATTSON
S IZVYEKOV
B RICE
D TAYLOR
N WEINGARTEN
RDRL WMP H
B AYDELOTTE
C MEYER
B SCHUSTER
D SCHEFFLER
RDRL WMM
J BEATTY
R DOWDING
M VANLANDINGHAM
RDRL WMM B
T BOGETTI
C FOUNTZOULAS
C DECKER
G GAZONAS
D HOPKINS
B LOVE
J O'GRADY
B M POWERS
T WALTER
R WILDMAN
C YEN
J YU
RDRL WMM D
A GAYNOR
B MCWILLIAMS
S WALSH
RDRL WMM E
J LASALVIA
RDRL WMM F
M TSCHOPP
RDRL WMM G
J ANDZELM
T CHANTAWANSRI
G J LENHART
C RINDERSPACHER
T SIRK
Y SLIOZBERG
RDRL WMP
S E SCHOENFELD
RDRL WMP B
S SATAPATHY
M SCHEIDLER
A SOKOLOW
T WEERASOORIYA
RDRL WMP C
R BECKER
S BILYK
T W BJERKE
D CASEM
J CLAYTON
M GREENFIELD
B LEAVY
J LLOYD
C MEREDITH
S SEGLETES
A TONGE
C WILLIAMS
RDRL WMP D
R DONEY
C RANDOW
S SCHRAML
M ZELLNER